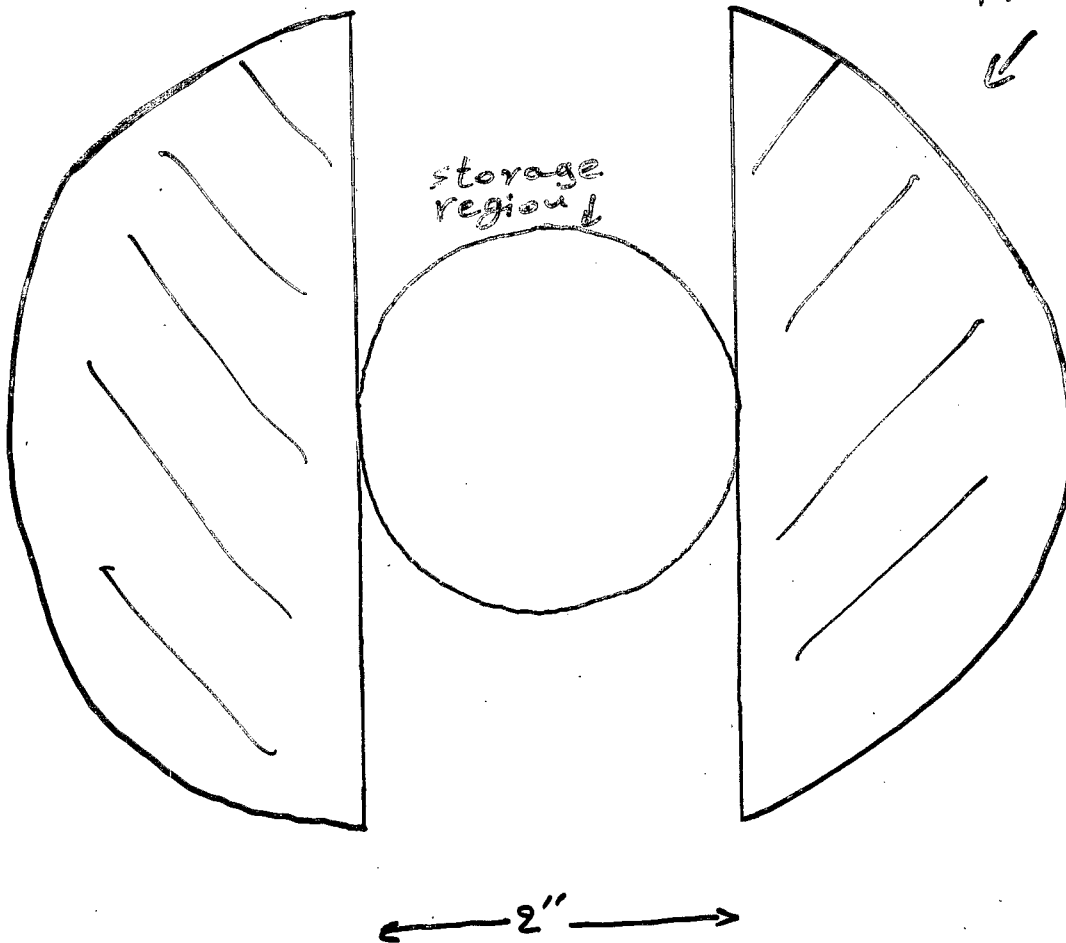


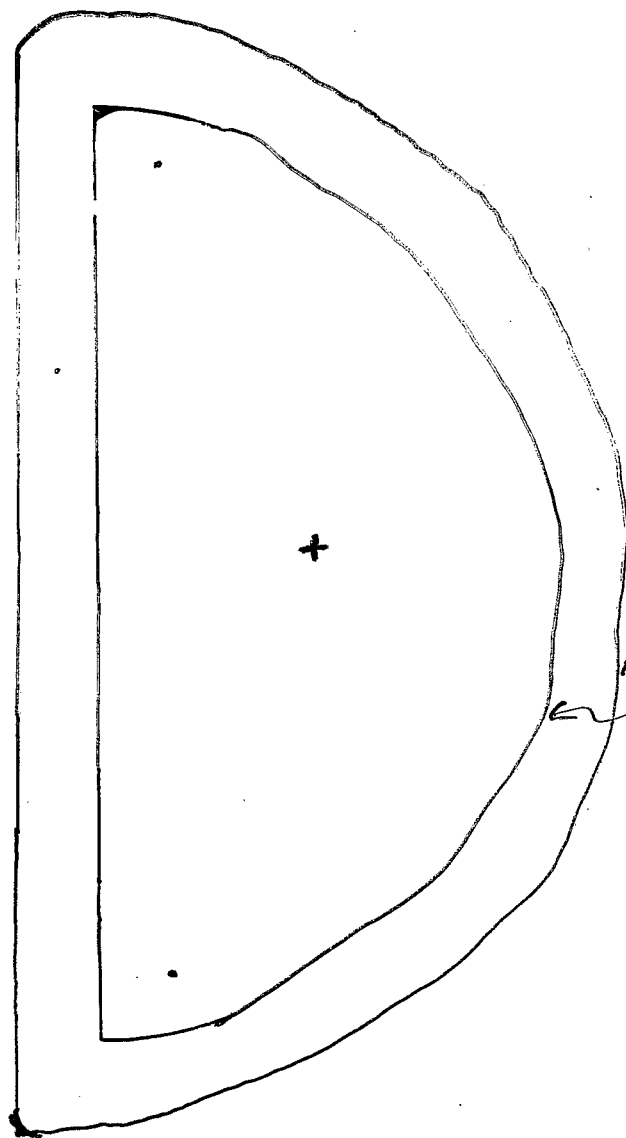
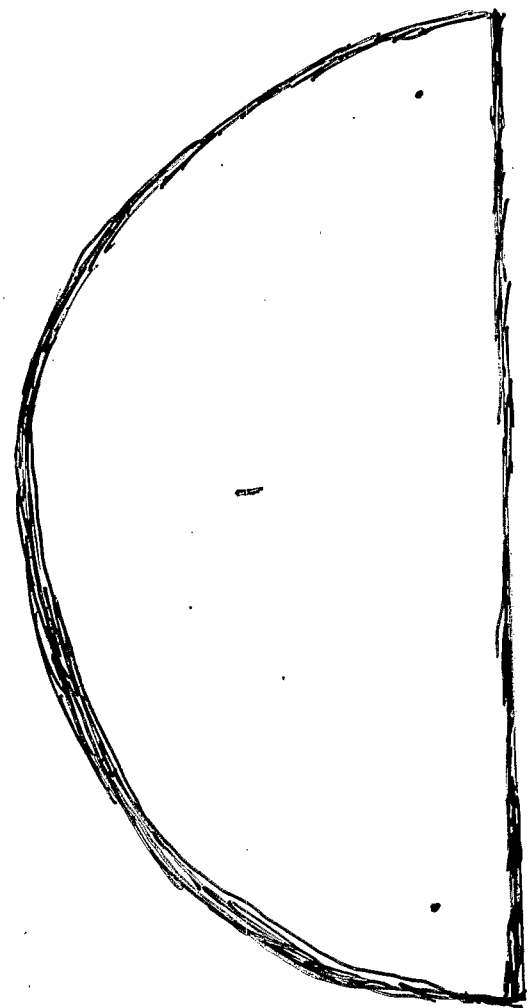
2/11/2003

YKS

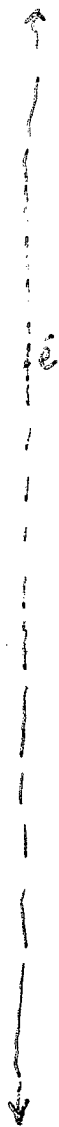
Low Energy Electron Trapping Issues.

Cross section of
Radial E-field
Plates

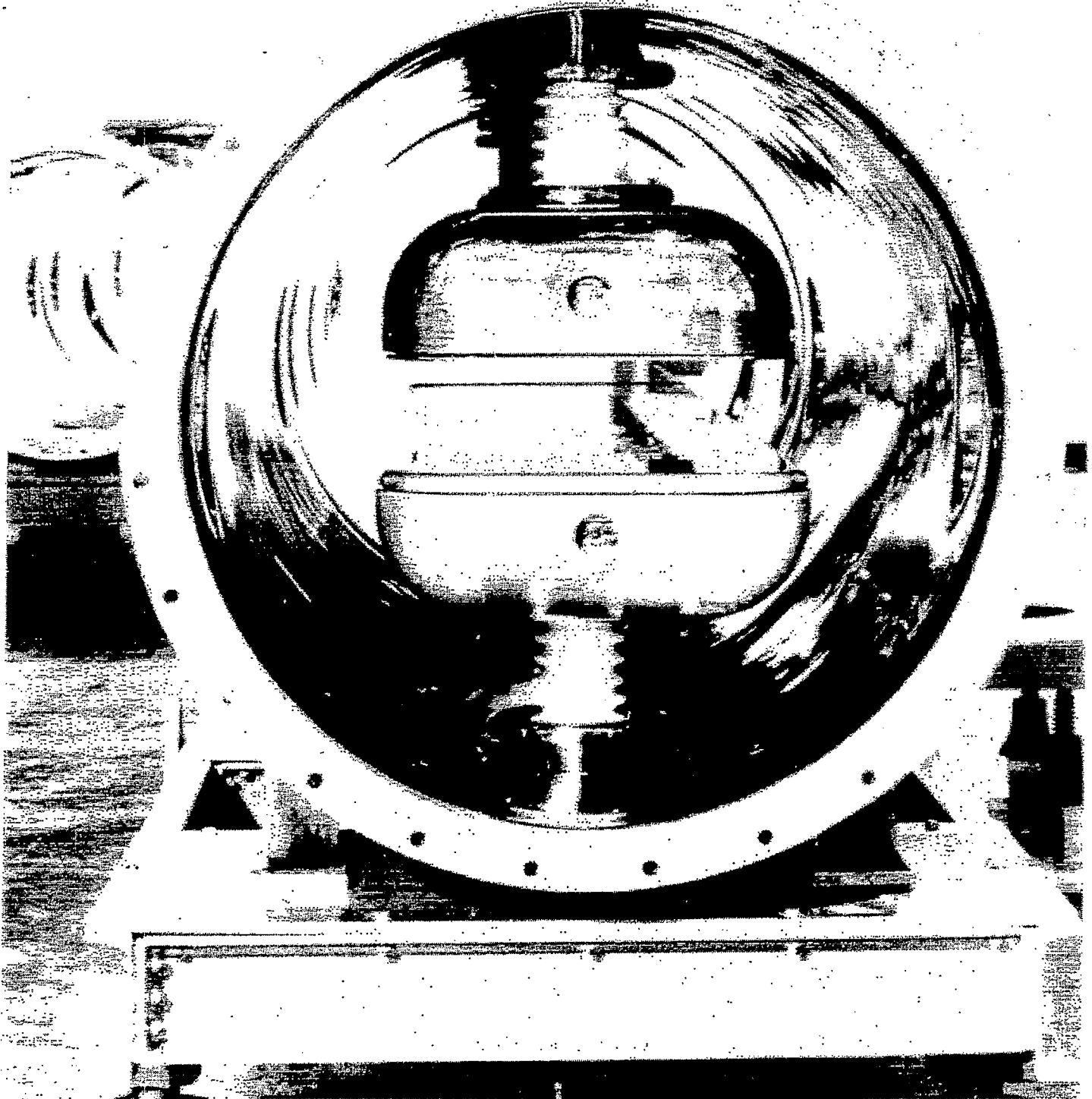




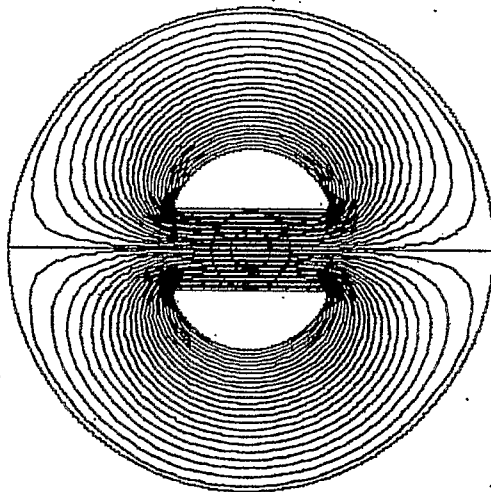
← equipotential
lines

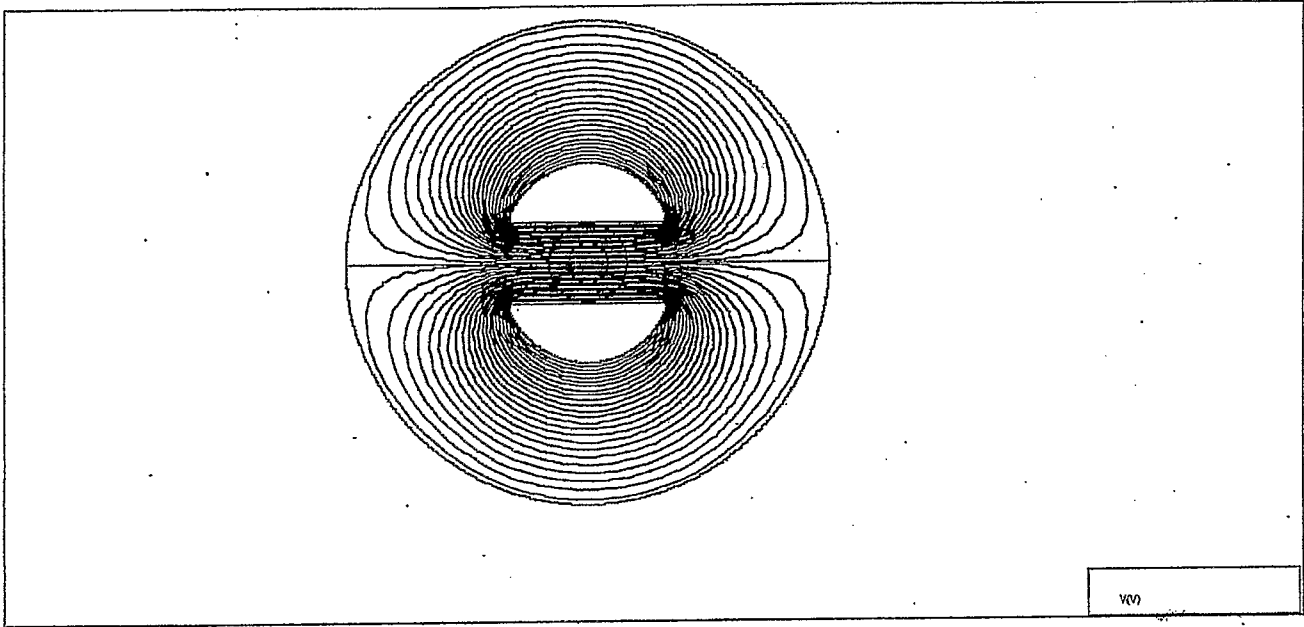


ENCLOSURE



00A





100

$$A_z = |z_0|$$

$$\langle \dot{y} \rangle_{av} = x_0 \omega_B \omega_E^2 / (\omega_B^2 - \omega_E^2) = 1.4 \times 10^7 x_0 \text{ ms}^{-1}$$

Note that the drift velocity is derived from $m\dot{y} + eBx = \text{constant} = +eBx_0$. It may also be shown that $\langle \dot{y} \rangle_{av} = -\langle E_x \rangle_{av} / B_z$, the well-known drift velocity of charged particles in crossed electric and magnetic fields.

In the non-stable cases electrons or ions can make a few oscillations before they hit the walls of the tank or the electrodes. The impact energy depends largely on the initial conditions, but in all these cases secondary emission of all sorts can occur.

From the above analysis we draw the following conclusion. Assuming that the rest gas contains none

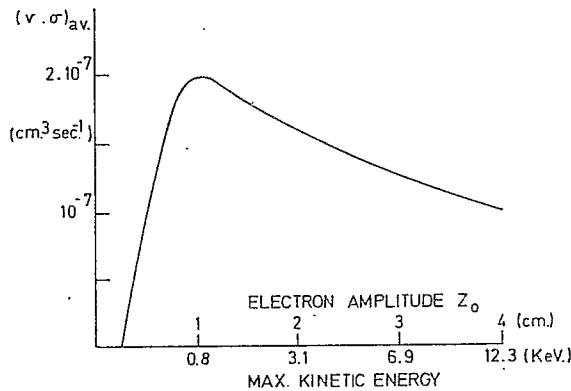


Fig. 8. Time average product of electron velocity and ionization cross section in nitrogen vs electron amplitude.

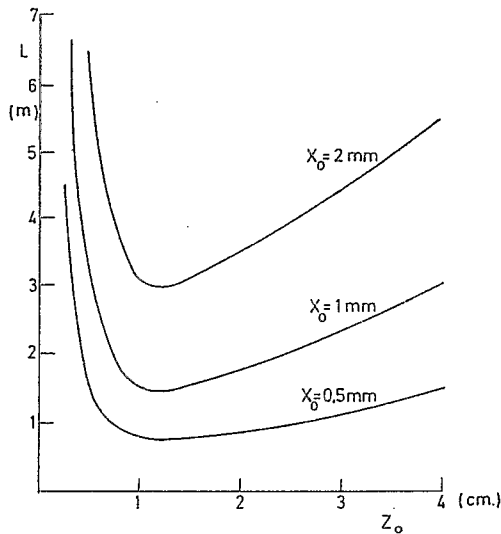


Fig. 9. Azimuthal collision length vs starting coordinates of the electron.

of the lighter elements, but some free electrons to start with, the only case for factual trapping is that in which the high-voltage electrodes are positive with respect to the low-voltage electrodes. Even so, the probability for ionization over a drift length of several metres is small. We will calculate this.

The vacuum we can reasonably obtain is of the order of 10^{-6} torr and the most probable rest gas will be nitrogen, so that the number of N_2 molecules is $n = 3.3 \times 10^{10} \text{ cm}^{-3}$. In the interesting case of electrons and positive V , we will calculate the lifetime τ and the drift length L for ionizing collisions as a function (x_0, y_0) of the electron at rest, using $\tau n \langle v\sigma \rangle_{av} = 1$. In this calculation we must time-average the product of the electron velocity v and the cross section σ . We readily verify that most (to 1%) of the kinetic energy of the electron goes in the z motion hence $v = \omega_E z_0 \sin \omega_E t$. Using cross-section data⁶ we obtain $\langle v\sigma \rangle_{av}$ as a function of z_0 (fig. 8). Over a lifetime τ , ranging typically from $150 \mu\text{s}$ to $300 \mu\text{s}$, the electron will drift in the axial direction by the amount $L = \tau \langle \dot{y} \rangle_{av}$. But $\langle \dot{y} \rangle_{av}$ is proportional to x_0 , resulting in fig. 9. Now the electrodes in the experimental set-up have a length $L_0 = 1.7 \text{ m}$, so that appreciable electron multi-

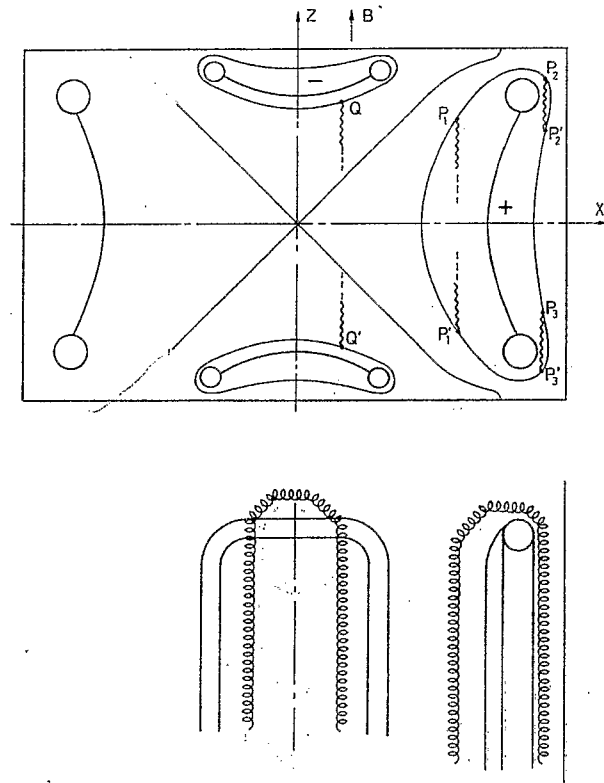


Fig. 10. Trapping of electrons for positive high voltage.

plication (interval $|x$ region on direct field able, and ionic impa build-up.

Indeed e into the q This can t us consid voltage ele surface is electron at only in the $H = T + e\phi$ on the field but it will a or more pr of the elec expect the up at the b regions (di where it ca P_3 . In wh starting-po because the velocity is l electron ag of its trav stand-off in in the med way.

A similar of electron motion is surfaces Q (see fig. 10 turn round other side respect the the old gec cannot exist

We have trons are un actual geo regions on permits tr surface arc appears th electron ini spiral betw

PULSED ELECTROSTATIC QUADRUPOLE FOCUSING FOR THE CERN MUON STORAGE RING

W. FLEGEL and F. KRIENEN

CERN, Geneva, Switzerland

Received 11 May 1973

In order to improve the precision in the measurement of the g -factor anomaly $a = (g-2)/2$, it is desirable to have the polarized muons circulating in a uniform magnetic field ($B \cdot v = 0$). Vertical focusing of the muons can be done with an electrostatic quadrupole field. Although the required potentials on the electrodes are reasonable (~ 40 kV), the combined action of magnetic and electric field considerably enhances the probability

of breakdown. This is due to trapped electrons which circulate around the electrodes and ionize the molecules of the rest gas. However, with reasonable vacuum ($< 10^{-6}$ torr) the build-up of charge is slow. Therefore a pulsed electrostatic quadrupole field is applied, the field being on during the storage time of the muons, i.e. 1 ms. In this way the system is operational.

1. Introduction

The principle of the $(g-2)$ experiment, in which this device is to be used, is to trap polarized muons in a uniform magnetic field ($B \cdot v = 0$) and measure the precession frequency ω_a of the spin relative to the momentum vector¹). The frequency is related directly to the g -factor anomaly $a = (g-2)/2$ through $\omega_a = a\omega_0$, in which $\omega_0 = eB/m$ is the cyclotron frequency of the muon at rest. MKS units are used.

The gradient component of the magnetic guiding field in a conventional weak focusing storage ring sets a limit to the accuracy with which the g -factor anomaly can be determined. In order to store enough muons in the ring, one needs both momentum spread and angular acceptance. Momentum spread means a spread in the radius of the equilibrium orbit $\delta p/p = \delta r/r$. Angular acceptance is proportional to the focusing strength of the magnet $n = -(r/B) \delta B/\delta r$. It follows that the muons can never move in the same average

field, namely $\delta B/B = -n\delta p/p$. Hence ω_0 is not the same for all muons. By averaging the frequencies on both sides, $\bar{\omega}_a = a\bar{\omega}_0$, the accuracy can still be quite good: in the previous experiment^{2,3}) $\bar{\omega}_0$ could be determined in the early stages of the storage via the average radius of the bunched rotating muon population to 160 ppm. However, the muon population could have changed at later times, either because of losses or of non-linear effects.

In the present experiment, B is constant and ω_a is independent of radius. The focusing is now achieved with an electrostatic quadrupole field. In general an electric field also affects ω_a , but at the so-called "magic muon energy"²) given by $\gamma^2 = a^{-1} + 1$ or $\gamma = 29.3$ the electric field does not influence ω_a . The corresponding muon momentum is then 3.098 GeV/c.

The focusing strength may now be written ($v =$ particle velocity) $n = rv^{-1}B^{-1}dE_r/dr$. The linearized equations for vertical (z) and radial (x) motion in a curvilinear set of coordinates will be $d^2z/ds^2 + nz/r^2 = 0$ and $d^2x/ds^2 + (1-n)x/r^2 = 0$, in which s is measured along the equilibrium orbit and r is the radius of curvature = 7 m. Suitable design value for n would be $n = 0.185$, i.e. half way between two resonances:

$$Q_x - 2Q_z = 0 \quad \text{or} \quad n = 0.2$$

and

$$2Q_x - 2Q_z = 1 \quad \text{or} \quad n = 0.1693.$$

Q_x and Q_z are the numbers of betatron oscillations per revolution for the horizontal and the vertical motion, respectively. The corresponding electric field gradient in this case would be $dE_r/dr = 1.17 \times 10^7 \text{ Vm}^{-2}$ for $B = 1.472$ tesla.

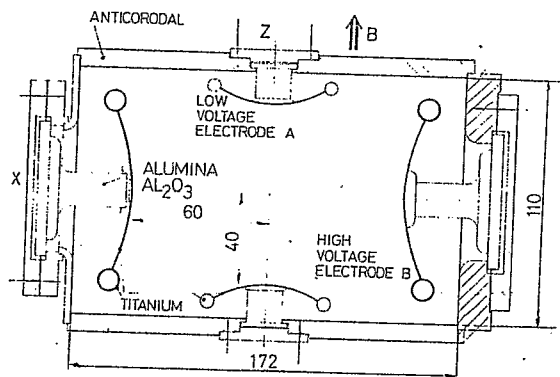
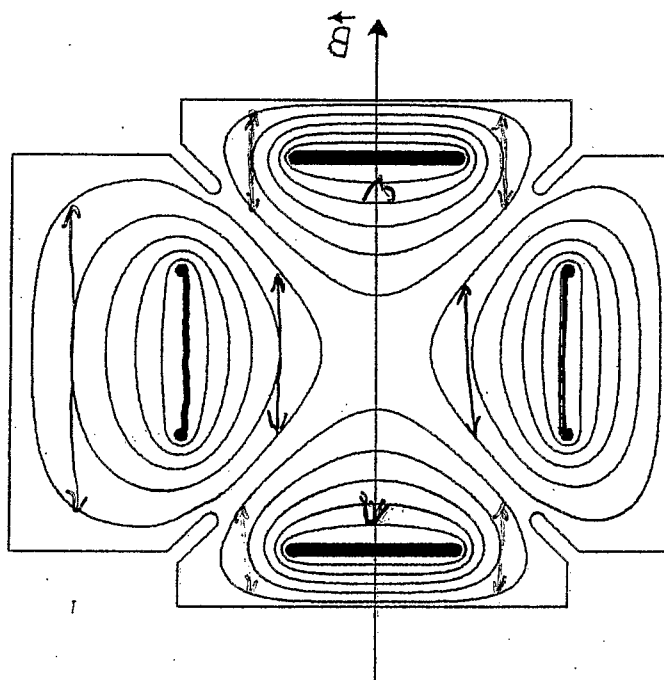
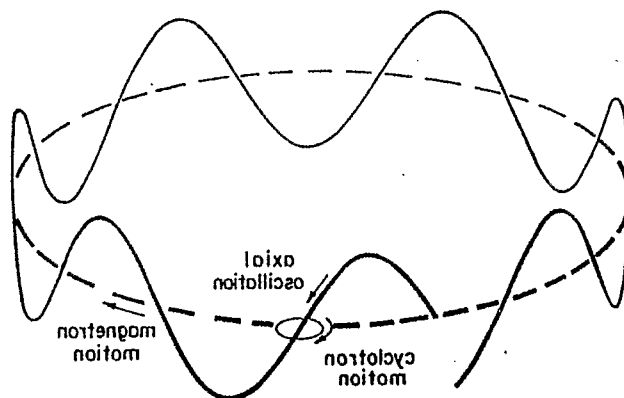
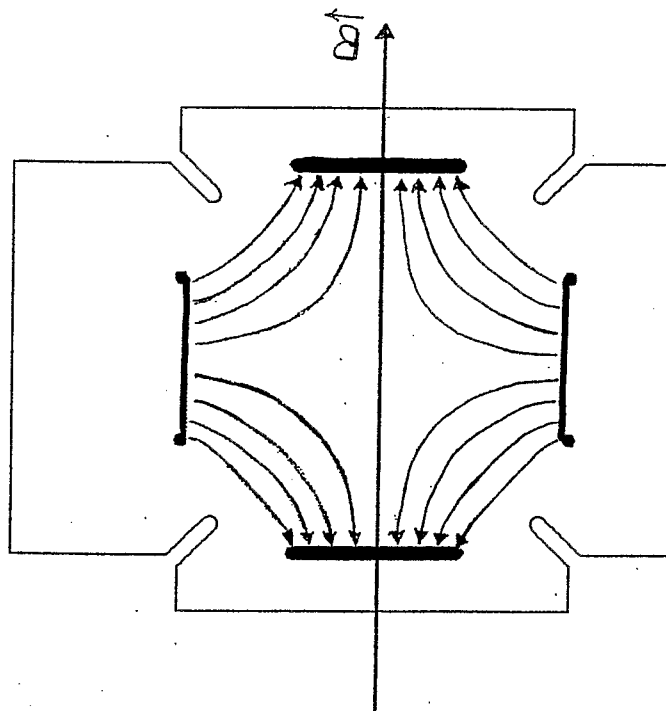


Fig. 1. Section of electrostatic quadrupole — final version.



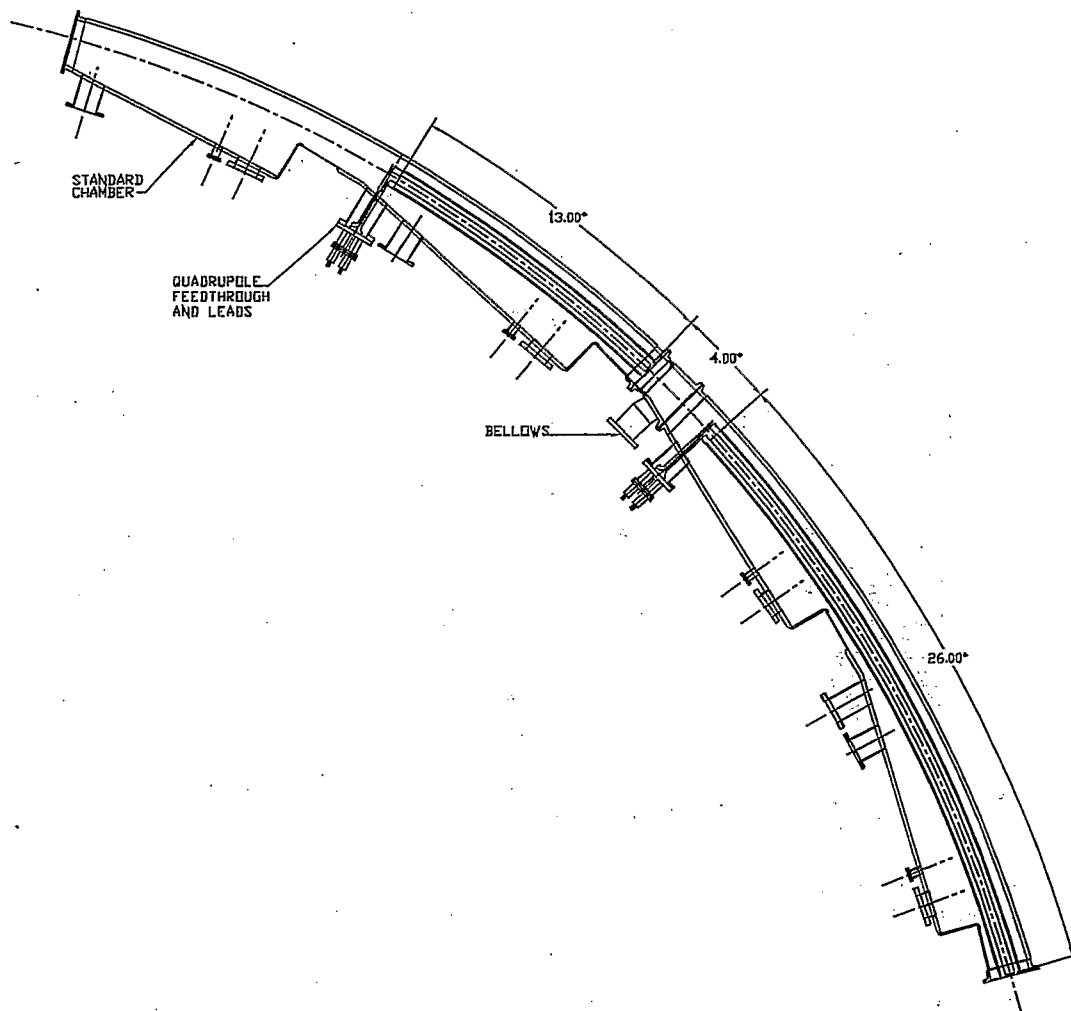


Fig. 7. Two consecutive vacuum chambers housing a quadrupole section. The upstream chamber houses the short section with a length of 13° and the downstream houses the long section with a length of 26° .

wall-thickness with small drilled holes to eliminate virtual vacuum leaks. The air to vacuum feedthroughs are a standard 30 kV commercial design. Tube-to-electrode joints and tube-to-tube joints are made with 2 mm aluminum pins.

4.2. Quadrupole mounting and support

4.2.1. Support frame

Each 13° electrode is mounted at three support points to a 28° aluminum support frame. A plan view of the support frame is shown in Fig. 9. The upper and lower plates of the frame were CNC

machined to the storage ring radius. The rigidity of the frame comes primarily from the corner ground plane electrodes: two screwed to the upper plate and two to the lower plate. These ground electrodes were extruded shapes which were stretch-formed to the approximate radius. Fifteen bars join the upper and lower assemblies. The support frame was accurately assembled on a flat surface.

Two of the support frame ground electrodes also serve as rails for a trolley containing the NMR magnet field measurement probes. The inner, lower rail has guide wheels for the trolley drive cable, visible in Fig. 6.

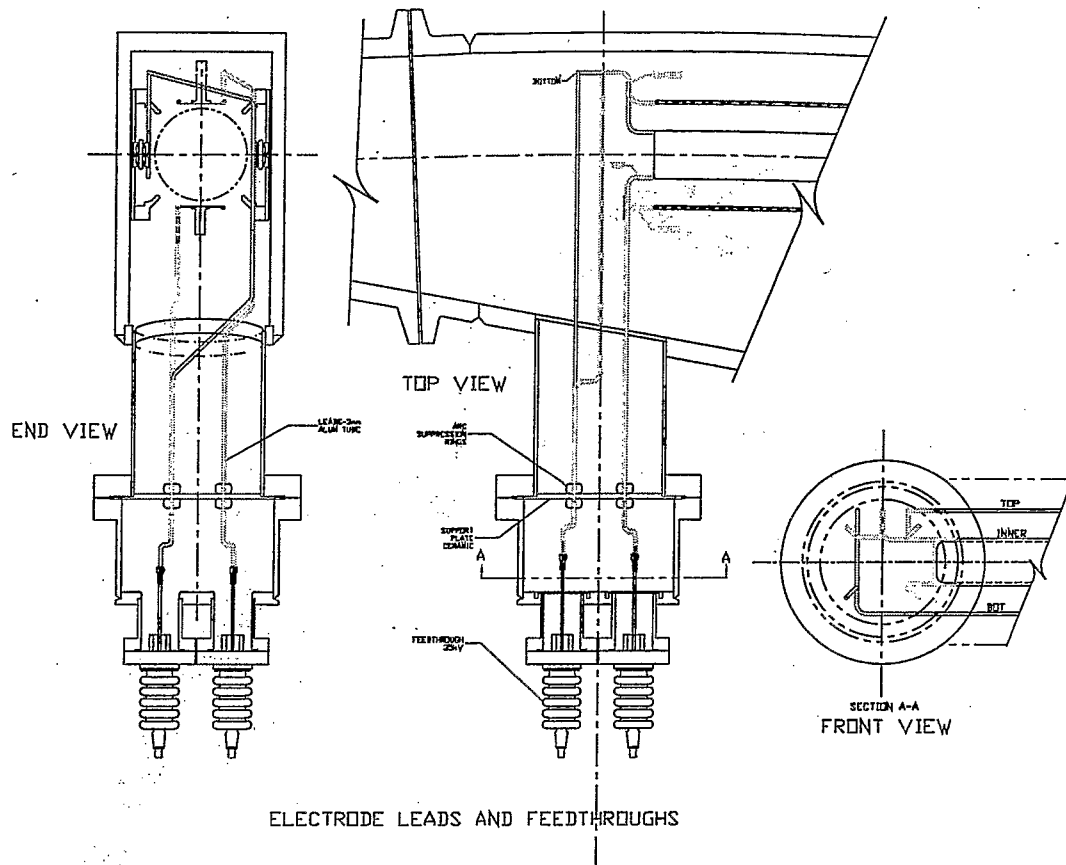


Fig. 8. The leads connected with the quadrupole plates are shown in different views. The maximum azimuthal extent of the leads is less than 10 cm from the end of the plates. The high voltage feedthroughs are also shown.

4.2.2. Electrode mounting

Each 13° electrode is attached to the support frame at three points using electrical isolators. The isolators for the upper and lower electrodes are made of Macor ceramic bonded to aluminum end plates, see Fig. 5. The upper and lower electrodes are 1.1 cm from the closest ground surface. The inner and outer electrode isolators were also machined from Macor.

4.3. Electrode alignment

The alignment of the quadrupole electrodes was performed in the following steps:

- (1) Upper and lower electrodes were aligned relative to the accurately CNC machined

inside diameter of the support frame plate. Inner and outer electrodes are vertically aligned relative to the lower electrode. The flexible inner and outer sheet metal electrodes are shimmed into the correct radius relative to the upper and lower electrode radial position. Acrylic gauge blocks were made for these alignments.

- (2) The vacuum chamber is "characterized" geometrically using a computer interfaced theodolite system (i.e., ManCAT). The chamber end flanges and targets on the inside radius define an external reference for the chamber dimensional database.
- (3) The support frame is installed into the vacuum chamber relative to the chamber end flanges. Adjusting screws on the frame

the four periods for the C/J analysis is 139.79 ± 5.12 indicated by the solid line and consistent with the values given in table 1. The estimated $\chi^2 = 4.58$ for 3 d.o.f which corresponds to 20% of C.L., i.e. they are self consistent.

Now we are ready to compare the 4th period between the C/J and Axel's results. Even though the total number of positrons between the two analyses in that period is close, it is estimated that the fraction of Axel's data which make it in the C/J analysis is only $79 \pm 1\%$ as discussed above. Using Eq. (1) with $\sigma_1 = 6.53$ ppm, $\sigma_2 = 6.18$ ppm, and $f_{12} = 0.79$ we get $\sigma = 3.67$ ppm, i.e. $\Delta R_4 = 2.54 \pm 3.67$ ppm. This is a 0.69 ppm which corresponds to 49% C.L.. Since the agreement is excellent we will take the weighted average of the two numbers which is: $R_4 = 132.9 \pm 6.18$ ppm.

In figure (2) I give the comparison of the R values of the different periods. The average of the four periods for the C/J/A analysis is 138.37 ± 4.95 indicated by the solid line. The estimated $\chi^2 = 5.0$ for 3 d.o.f which corresponds to 18% of C.L., i.e. they are self consistent.

The final numbers per period and their average is given in table 6. Finally in figure (3) I give the distribution of the C.L. of the tests and comparisons I applied in the analysis of the four periods. Those are the comparisons between Cenap's and Joerg's results (4 points, see table 4), the comparison between Axel's result and C/J for the fourth period (49%), and the C.L. from the comparison of the R value distribution from the four periods (see figure (2)). The average is 56%, slightly above the expected value of 50%.

6 ω_p Analysis

The magnetic field analysis was mainly done by Ralf Prigl and H. Deng. Klaus Jungmann, Alex Grossmann have contributed in the analysis in many different ways, and Vernon Hughes has contributed in the assignment of the B-field systematic errors. Sergei Redin has estimated the average B-field with both, beam tracking and analytically (assuming a certain muon distribution). He found that only the dipole and quadrupole components are important and the average is estimated equally well with tracking and analytically.

The ω_p analysis group had weekly meetings at BNL to follow the progress.

pole electrode lengths of the short and long plates are approximately 1.6 and 3.2 m, correspondingly. When the trapped electrons reach the end

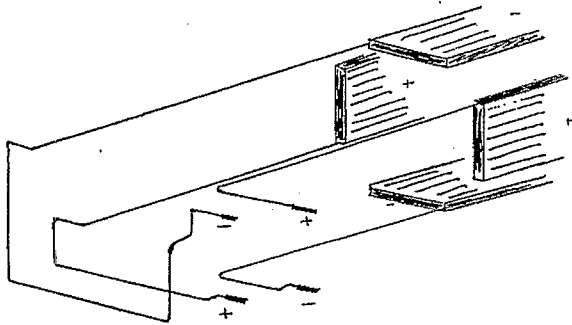


Fig. 11. A three dimensional representation of the quadrupole leads is shown in this schematic (not to scale). The lead geometry is such that the up/down, left/right symmetry is broken. The azimuthal extent of the leads is less than 10 cm.

of the plates the electric field shape is such that they re-enter the quadrupole region [14]. Therefore for a trapped electron 1 cm away from the center, it takes approximately 50 and 100 μs for the short and long plates, respectively, to travel the length of the quadrupole plates and return to the same point.

The electron trapping occurs because the electrostatic quadrupoles combined with the vertical dipole B -field form a local penning trap for low energy particles. The fact that at the end of the quadrupole plates they return into the quadrupole region is due to the symmetry of the electric fields. We decided to break this symmetry at the one end of the plates by designing the quadrupole leads in a way that the quadrupole electric field is rotated by approximately 25° (see Figs. 8, 11, 12). The azimuthal extent of the leads is less than 10 cm

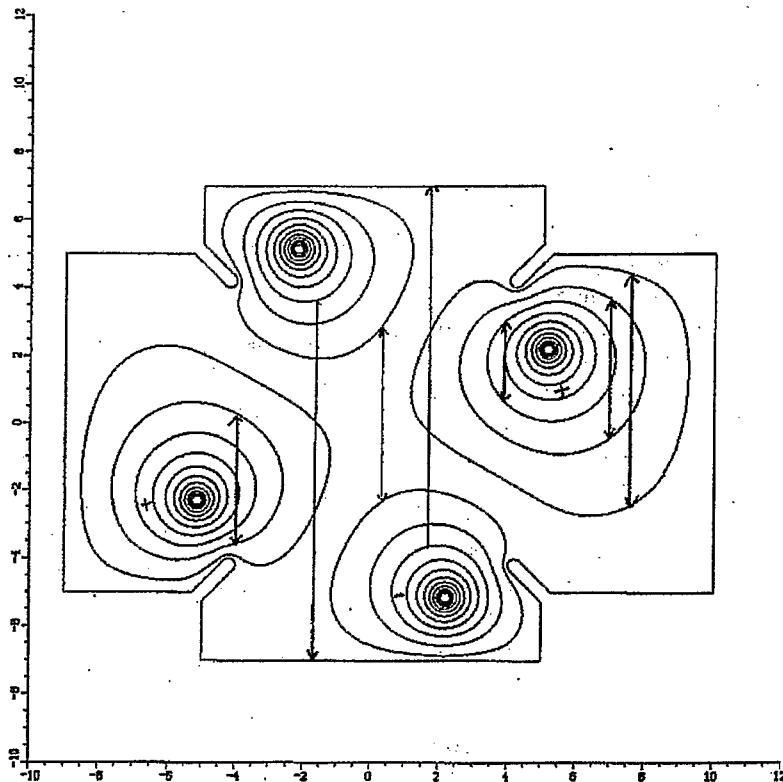
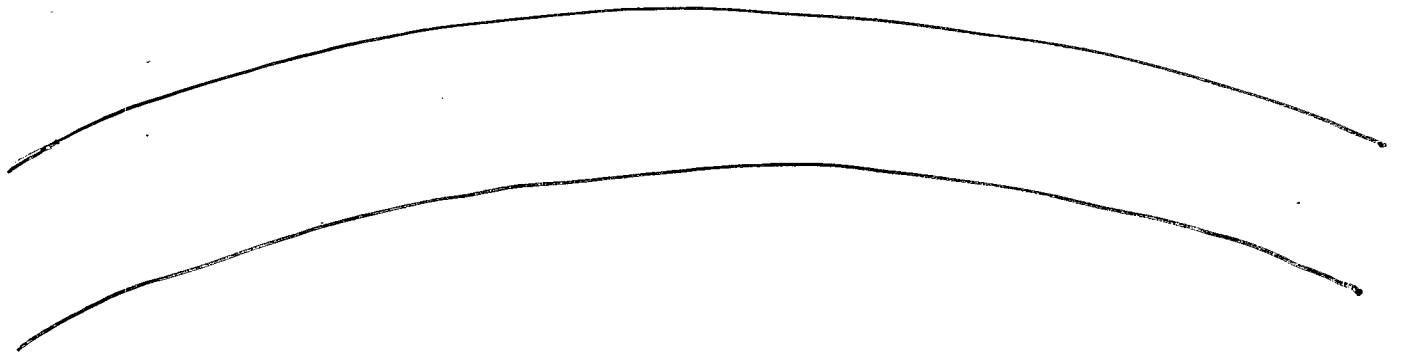
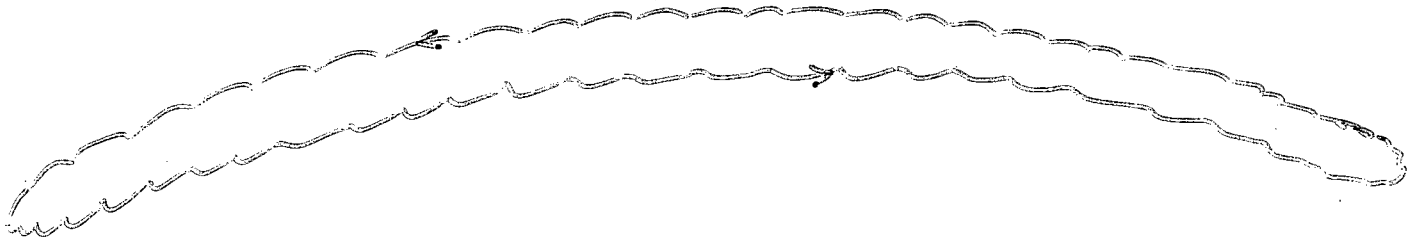


Fig. 12. The cross section of the leads, the trolley rails as well as the equipotential lines are shown. The vertical lines indicate the vertical motion of the trapped electrons at the lead location for the negative muon storage polarity. The trapped electrons that end up in the positive leads (left/right in this polarity) are eventually driven out to the feedthrough region due to the $\vec{E} \times \vec{B}$ drift. Most of the trapped electrons that end up in the central region are released while a small fraction remains captured. The units in the horizontal and vertical axes are in cm.

Top View of ϵ -field Plates



an e^- path



- charge buildup \rightarrow sparks

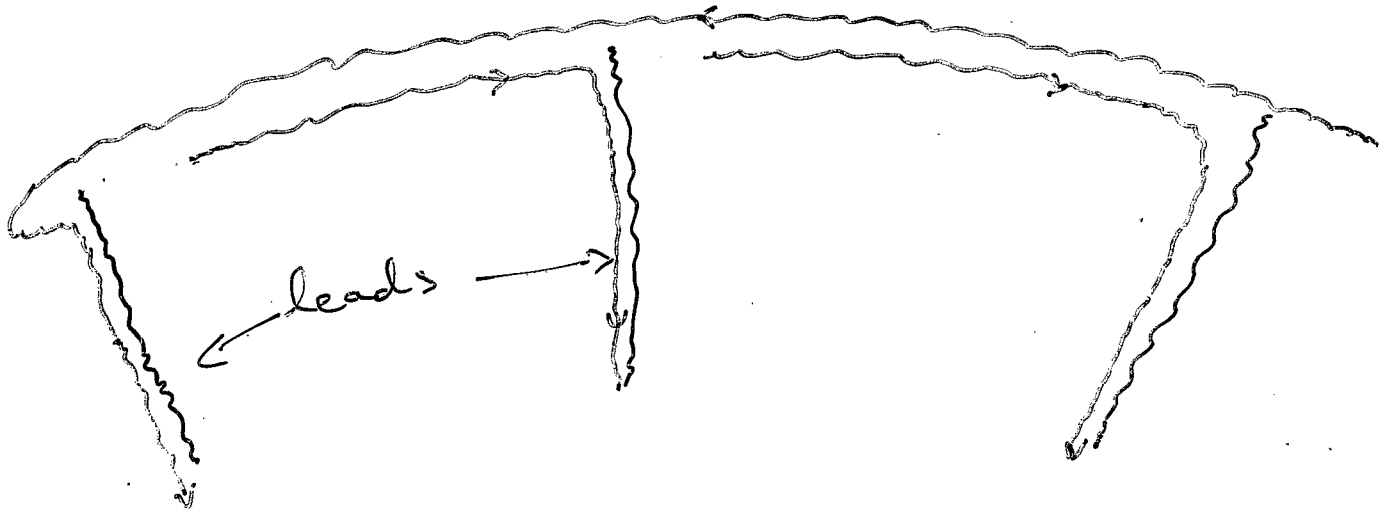
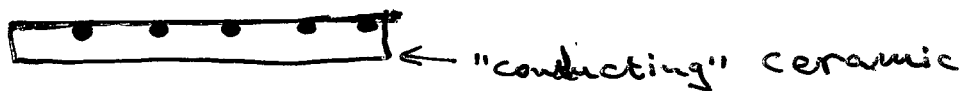
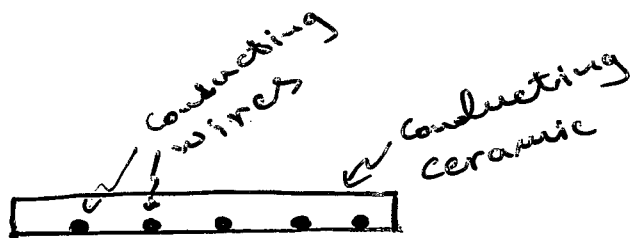


Table 7: The final numbers (ω_a) with their corrections.

<i>Name</i>	ω_a [Hz]	Error [ppm]	E cor. [ppm]	Pitch [ppm]	Final ω_a [Hz]
C/J/A	229068.299 (with an offset)	4.95	-0.50	-0.29	229068.118 ± 1.134 (with an offset)

Table 8: The final numbers (ω_p) with their corrections.

<i>Name</i>	ω_p [Hz]	Error [ppm]	B_{Quad} cor. [ppm]	Final ω_p [Hz]
R/D	61789661.6 (with an offset)	0.53	-0.21	61789648.6 ± 32.7 (with an offset)



e^- will be collected by the ceramic (thin layer).
Desirable time constant $\tau \sim 1 \mu s$.

AN ELECTROSTATIC SEPARATOR WITH BUILT-IN HIGH-VOLTAGE GENERATORS

AKIRA YAMAMOTO, AKIHIRO MAKI and ASAO KUSUMEGI

National Laboratory for High Energy Physics, Oho-machi, Tsukuba-gun, Ibaraki, 300-32, Japan

Received 9 December 1976 and in revised form 23 May 1977

An electrostatic separator with high-voltage generators mounted directly onto the separator chamber is described together with the present performance of the separator of this type. A maximum voltage of 900 kV was obtained with the 3 m separator and of 800 kV with the 9 m separator for an interelectrode spacing of 10 cm.

1. Introduction

In the field of high-energy physics, electrostatic separators have been used extensively for the separation of secondary particles with momenta below approximately $6 \text{ GeV}/c$ ^{1,2}). A conventional way to supply high-voltages across the electrodes of electrostatic separators is to use special cables between the high-voltage generators and the electrodes through lead-in bushings³). This method of using high-voltage cables results in considerable technical problems, such as insulation of cables, complex end treatments with stress cones and oil treatments when connecting or disconnecting the cables.

The high-voltage applied to the electrode of the separator is several hundred kV and therefore, in general, the size of the cable becomes large, 5–10 cm diameter. The heavy weight and the bulky stress cones at the terminals for both shielded and unshielded cables make the handling of these cables tedious and cumbersome. If unshielded cables were used to reduce the capacity of high-voltage cables, sparks along the cable surface cause operational problems, namely, severe electrical noises and damages to the equipment. An attempt had been made at Argonne to eliminate high-voltage cables by charging the electrode to the required potential with an energetic electron beam⁴). This technique has proved to be impractical, however.

We have solved these problems entirely by mounting the high-voltage generators directly onto the vacuum chamber. As a result, no high-voltage appears outside the vacuum chamber. An additional benefit that has been realized later is that the stored energy is much less for this type of separator than for conventional ones with high-voltage cables that inevitably add more capacitance to the system. Therefore, the spark damage to the

electrodes and insulators is minimized. We obtained a maximum voltage of 900 kV with a 3 m separator and of 800 kV with a 9 m separator across a gap spacing of 10 cm. We have operated these separators for several months and we anticipate further improvement mainly by additional conditioning.

2. Configuration of the KEK electrostatic separator

2.1. HIGH-VOLTAGE POWER SUPPLY

A compact high-voltage power supply has been developed and manufactured for the KEK elec-

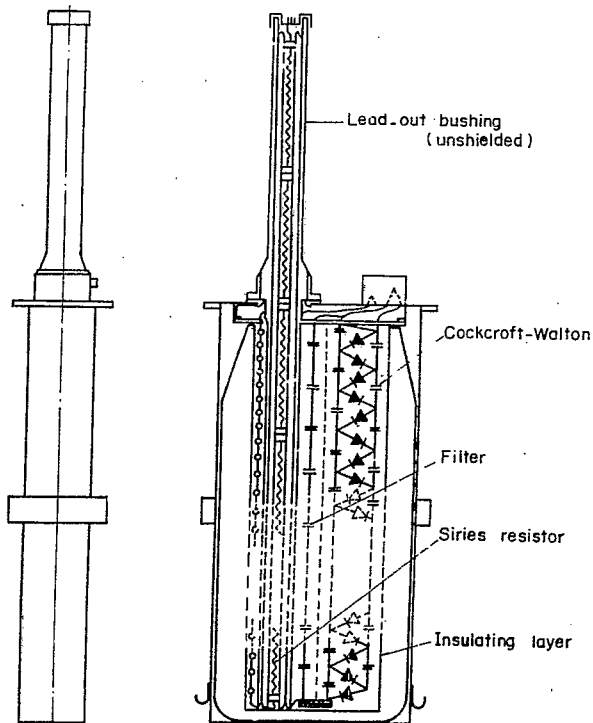


Fig. 1. Schematic diagram of the high-voltage generator.

9 m separator is shown in fig. 4.

3. Present operation and performance

A series of tests was performed on a model separator and the 3 m separator to obtain as high a maximum voltage across the electrodes as possible⁶). These tests were: (1) test of the components, particularly, of lead-in bushings and support insulators, (2) the effect of conditioning, (3) the effect of the type of gas, (4) the effect of the electrode material, (5) the dependence on polarity, (6) the effect of deconditioning and (7) the effect of the dimensions of components and others. The results

voltage was 800 kV across the electrodes. The sparking rate was ~ 5 sparks per hour at 800 kV. It went down to ~ 1 spark per hour at 750 kV and ~ 2 sparks per day at 700 kV. The deconditioning rate was approximately the same as that of the 3 m separator.

4. Conclusion

We have presented the results of the operation and performance of the 3 m and 9 m KEK electrostatic separators together with their design details. We believe that the separators with the built-in high-voltage generators are superior to those with conventional high-voltage cables. Many

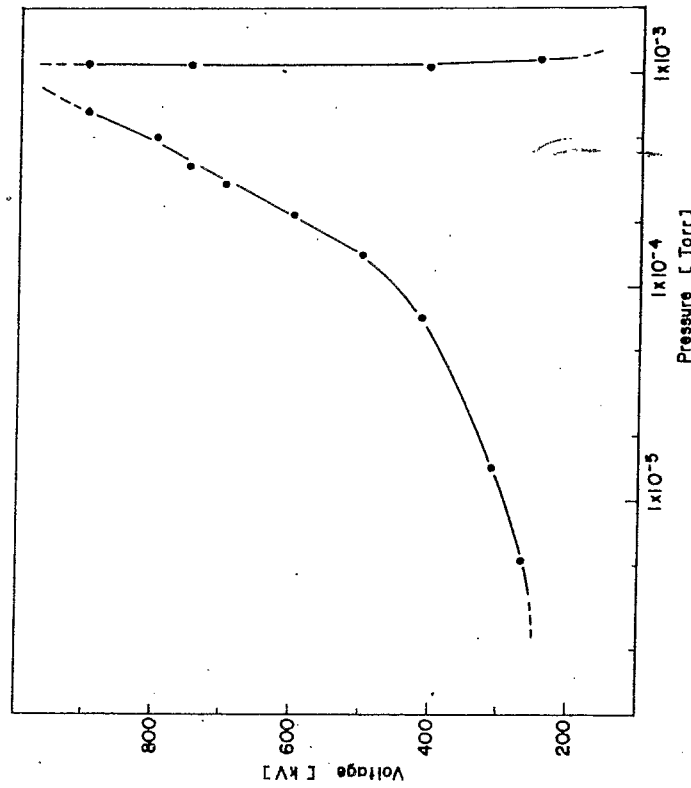


Fig. 5. Performance of the 3 m separator. High-voltage is supplied between stainless-steel anode and anodised aluminium cathode. The gap spacing is 10 cm. A gas mixture of neon and helium (36.5%) is used to adjust the working pressure. Pressures are "equivalent nitrogen".

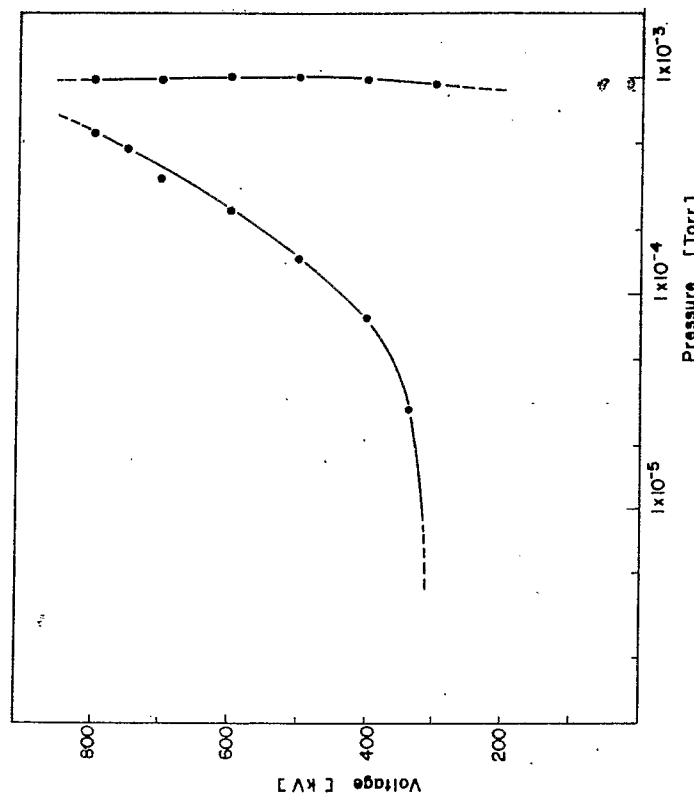


Fig. 6. Performance of the 9 m separator. The conditions of the electrodes, gas mixture and gap spacing are the same as those of the 3 m separator. Pressures are "equivalent nitrogen".

Comments:

— w/ He gas low energy trapped e^-
lose energy by collisions — don't ionize.

⇒ we may be able to ~~offset~~ turn on
the inside of the plates.

Need to test...

— E-field plates longer than B-field
region by ~5 cm.

— A combination of wires and conducting
ceramic could collect away the δ -rays.

Need to test...